SUPPLEMENTARY ONLINE INFORMATION FOR:

Structural coupling of the EF hand and C-terminal GTPase domains in the mitochondrial protein Miro

Julian L. Klosowiak[1], Pamela J. Focia[2], Srinivas Chakravarthy[3], Eric C. Landahl[4], Douglas M. Freymann[2], Sarah E. Rice[1+]

[1]Department of Cell and Molecular Biology, [2]Department of Molecular Pharmacology and Biological Chemistry, Feinberg School of Medicine, Northwestern University, 303 East Chicago Avenue, Chicago, IL 60611, USA, [3]Biophysics Collaborative Access Team, Advanced Photon Source, Argonne National Laboratory, 9700 S. Cass Avenue, Argonne, IL 60439, USA, [4]Department of Physics, DePaul University, 2219 N. Kenmore Avenue, Chicago, IL 60614, USA.

[+]Corresponding author. Tel: +1 312 503 5390; Fax: +1 312 503 7912; E-mail: s-rice@northwestern.edu

SUPPLEMENTARY METHODS

Cloning, expression and purification of Miro. The *Drosophila* dMiro$_{1-617}$-6xHis isoform D (MiroL) was purified as described previously [12]. The dMiro$_{201-617}$-6xHis isoform D (MiroS) coding sequence was PCR amplified from a full-length cDNA construct (Drosophila Genomics Resource Center clone RE22983), and subcloned into Nde1 and EcoRV sites in a modified pET17b(+) vector (C-terminal 6xHis-tag, Novagen). The construct was verified by DNA sequencing. Numbering corresponds to full-length dMiro isoform D. MiroS was expressed in *E. coli* BL21-CodonPlus® (DE3)-RP cells (Stratagene) cultured in TPM medium at 37 °C to OD_{600} = ~1.0, cooled to 18 °C and induced with 125 μM IPTG for ~16 h. For selenomethionine (SeMet)-substituted MiroS, cells were cultured in M9 minimal medium (Medicilon) using the method of methionine biosynthesis feedback inhibition [32]. All further steps were conducted at

4 °C unless otherwise noted. Cells were pelleted at 5500 rpm for 13 min in a JA-10 rotor (Beckman Coulter), re-suspended in a minimal volume of resuspension buffer (25 mM HEPES at pH 7.4, 300 mM NaCl, 0.5 mM TCEP, 20 mM imidazole, 1 mM EGTA, 0.5 mM $MgCl_2$, 20 µM GTP, 0.02% Tween, 1 mM PMSF, 2 µg/mL Aprotinin, 4.7 µg/mL Leupeptin, 0.7 µg/mL Pepstatin A), flash frozen by dripping drop-wise into liquid N_2 (LN_2), and stored at - 80 °C. Cells were then thawed in a 37 °C water bath, lysed by sonication, and pelleted at 35,000 rpm for 45 min in a Ti45 rotor (Beckman Coulter). The cleared lysate was incubated with nickel-agarose beads (Ni-NTA Agarose, Qiagen) for 1 h, washed using Ni-buffer (resuspension buffer lacking protease inhibitors) supplemented with 60 mM imidazole, and eluted using Ni-buffer supplemented with 300 mM imidazole. Bradford-positive fractions were pooled, diluted ~four-fold with buffer A (25 mM HEPES at pH 7.4, 0.5 mM TCEP), loaded onto a HiTrap SP HP cation-exchange column (GE Healthcare), and eluted with a linearly increasing salt gradient of buffer A mixed with buffer B (25 mM HEPES at pH 7.4, 0.5 mM TCEP, 1 M NaCl). Purity of MiroS was confirmed by SDS-PAGE and/or SEC-MALS. For SAXS studies, the relevant fractions were pooled, supplemented with 20% sucrose, and flash frozen by dripping into LN_2. For crystallization trials, the relevant fractions were pooled and dialyzed in 10,000 MWCO dialysis cassettes (Thermo Scientific) for ~ 16 h in crystallization buffer (25 mM HEPES at pH 7.4, 0.5 mM TCEP, 0.5 M NaCl). The dialyzed protein was spin concentrated using a 50 K MWCO spin concentrator (Amicon Ultra, Millipore) to ~ 5-15 mg/mL as measured by A_{280} using an extinction coefficient of 54,320 $mol^{-1}cm^{-1}$ and a molecular weight (MW) of 49,047 Da for MiroS. An extinction coefficient of 71,740 $mol^{-1}cm^{-1}$ and a MW of 71,008 Da was used for MiroL. Extinction coefficients and MWs were determined from primary amino acid sequences using the online ProtParam tool: http://web.expasy.org/protparam/. Finally, the protein solution

was cleared of aggregates by ultracentrifugation at 100,000 rpm for 10 min in a TLA 110 rotor and Optima™ TLX ultracentrifuge (Beckman Coulter).

Crystallization. Crystals were grown using the sitting-drop vapor diffusion method at 21 °C with a drop size of 1 µL. Protein and reservoir solution was mixed in three different ratios: 2:3, 1:1, and 3:2, in Intelliplate 96-3 trays using a Phoenix robot (Art Robbins Instruments). Protein and reservoir solutions varied slightly between conditions that yielded crystals for the four structures and are listed here by structure. SeMet-MiroS (two crystals): 1) 1.5 M $LiSO_4$, 0.2 M Bis-Tris at pH 7.5 with 10.8 mg/mL MiroS and 2) 1.5 M $LiSO_4$, 0.1 M Bis-Tris at pH 8.0 with 4.5 mg/mL MiroS in crystallization buffer supplemented with 1mM $MgCl_2$ and 1mM GMPPCP. Apo-MiroS: 1.7 M $LiSO_4$, 0.1 M Bis-Tris at pH 7.6 with 5.0 mg/mL MiroS in crystallization buffer supplemented with 5 mM EGTA. Ca-MiroS: 1.7 M $LiSO_4$, 0.1 M Bis-Tris at pH 7.4 with 5.0 mg/mL MiroS in crystallization buffer supplemented with 5 mM EGTA. MgGDP-MiroS: 1.9 M $LiSO_4$, 0.1 M Bis-Tris at pH 8.0 with 5.0 mg/mL MiroS in crystallization buffer supplemented with 5 mM EGTA. Ca-MiroS and MgGDP-MiroS crystals were soaked in 10mM $CaCl_2$ and 30 mM $MgCl_2$ + 20 mM GDP, respectively, for ~72h prior to flash cooling in LN_2. All crystals were harvested directly from their mother liquor without added cryoprotectants.

X-ray diffraction data collection and structure determination. Measurement of X-ray diffraction data was performed at the beamlines of the Life Sciences Collaborative Access Team (LS-CAT) at Sector 21 of the Advanced Photon Source (APS) in the Argonne National Laboratory (ANL). Data were measured at 100K using a MarMosaic 225 CCD detector with an X-ray wavelength of 0.97872 Å, and were integrated and scaled using HKL2000 [33] or MOSFILM [34]. Diffraction from these crystals was notably anisotropic, limited in all cases to

~3.0 Å resolution in the h k plane. Resolution cutoffs were applied based on software estimates implemented in AIMLESS [34]. Crystals belong to the $P3_221$ space group. Data from two isomorphous SeMet crystals (see above) were merged to improve the completeness of the data for phasing by single wavelength anomalous dispersion (SAD). Phasing was carried out using Phenix [35], and 10 selenium atoms were located. An initial model obtained using Phenix AutoBuild comprised 375 of an expected 417 residues and revealed the overall domain structure. After inspection, rebuilding using COOT [36], and initial crystallographic refinement using Phenix, the SeMet structure was used as a search model in Phaser [37] to obtain by molecular replacement the apo-MiroS, Ca-MiroS, and MgGDP-MiroS structures described here. Crystallographic refinement was carried out with Phenix, which implements a default bulk solvent correction and anisotropic scaling of the data [38]. Crystallographic statistics for the four structures are presented in supplementary Table S1. The N-terminal six residues and the C-terminal 9 residues of the MiroS construct (201-617) are disordered in the crystal and were not located. In all structures a large loop comprising residues 434-441 in Lnk2 is poorly ordered, despite the sidechains of I435 and L437 contributing to a hydrophobic crystal contact (supplementary Fig 5B), and a second loop comprising residues 561-566 that follows GTPase sequence motif G4 is ordered only in the MgGDP-MiroS complex. Residues of both have been built as Ala or Gly where sidechain positions could not be determined. A well-defined electron density feature occurs at the core of the ELM1 helix bundle in each of the structures (Fig 2B, supplementary Figs S3 and S5). Based on the size and shape of the electron density and a survey of the PDB ligand database, we have modeled the feature as homoserine, but the resolution of the electron density maps is not sufficient to unambiguously identify it. Its origin, identity, and even whether it represents the ordered fragment of a larger molecule, remain

unknown. ELM1 cavity volume was calculated using the Pocket-Finder pocket detection server [39]. Buried surface area was calculated using the cocomaps server [40]. All figures were created in PyMol [41], Microsoft Excel (Microsoft Corp. Redmond, WA), and/or Adobe Illustrator (Adobe Systems Inc., San Jose, CA).

Structure and sequence alignment. Structure-based alignments were performed using the DALI server [42]. Sequence alignment was performed using ClustalW2 [43]. Identity and similarity of Miro sequences was determined using Supermatcher, which is available as part of the Mobyle project at: http://mobyle.pasteur.fr/cgi-bin/portal.py?#welcome. Supermatcher uses a Needleman-Wunsch algorithm for alignment. Gap creation penalty was 10, gap extension penalty 0.5. Angles between helices were computed using the angle_between_helices command in PyMol. Reported helical angles represent the average of three methods for helical angle determination: (1) using alpha-carbon positions, (2) using the orientation of the hydrogen bonds found within the helix, and (3) using all atom positions within the helix. Helical angles using these three methods agreed to within 8% or better.

Small Angle X-ray Scattering (SAXS). Solution SAXS experiments were performed at beamline 18-ID-B of the Biophysics Collaborative Access Team (BioCAT) at the APS in the ANL. Details of the beamline setup can be found in [44]. All steps were conducted at 4 °C unless otherwise noted. MiroS protein, prepared as described above, was thawed in a 37 °C water bath and then dialyzed for ~ 16 h in SAXS buffer (25 mM HEPES at pH 7.4, 300 mM NaCl, 0.5 mM TCEP) supplemented with either 1 mM EGTA (MiroS-apo), 1 mM EGTA + 1 mM $MgCl_2$ (MiroS-Mg), 1 mM EGTA + 1 mM $MgCl_2$ + 1 mM GDP (MiroS-MgGDP), or 3 mM $CaCl_2$ (MiroS-Ca), 3 mM $CaCl_2$ + 1mM $MgCl_2$ + 1 mM GDP (MiroS-Ca+MgGDP), 3 mM $CaCl_2$ + 1mM

$MgCl_2$ + 1 mM GTP (MiroS-Ca+MgGTP). The dialyzed protein was spin concentrated to ~ 1 mg/mL and cleared of aggregates by ultracentrifugation. MiroS solutions 200 µL in volume ranging from 0.1 – 1 mg/mL were loaded into a 1.5 mm diameter capillary located vertically in a capillary holder cooled to 10 °C. The capillary was centered in the X-ray beam and the solution was continuously cycled up-and-down to reduce radiation-induced damage as a total of 20 exposures, 0.5 s in duration, were measured. Buffer solutions matched to each Miro sample were measured in the same capillary prior to each experimental run. Photons scattered from the 12 keV X-ray beam were detected with a detector at a distance of 1.539 m from the sample. The 40 images, 20 each from buffer and sample sets, were radially binned to obtain I vs. q curves. The curves from each set were averaged after removal of statistical outliers. The resulting averaged buffer curve was subtracted from the sample curve. The radius of gyration (Rg) was determined by Guinier analysis. Where possible, the particle distribution function P(r) was determined using the program GNOM [45] to confirm the radius of gyration (Rg) and to determine the maximum diameter, Dmax. Error in Rg was calculated from weighted linear regression analysis of log(I) vs. q^2 from raw SAXS data. In determining Dmax, GNOM gives a "total estimate", which identifies common artifacts encountered by the GNOM method. The total estimates for MiroS-Ca and MiroS-Ca+MgGDP were good, and the total estimate for MiroS-Ca+MgGTP was reasonable. Good/reasonable total estimates indicate that commonly observed errors were not made in determining Dmax for our datasets. Scattering data of apo MiroS and MiroS in the presence of Mg^{2+} but not Ca^{2+} or nucleotide showed evidence of some unfolded and/or aggregated protein in the high and low Q range of the scattering curves. While these data were of sufficient quality to obtain Rg or Dmax, they were not used for SAXS reconstructions. Like other EF hand proteins, Miro may be less stable in the absence of Ca^{2+}

[14,21]. Dummy atom modeling for SAXS reconstructions was done with the program DAMMIF [46] (10 runs per SAXS structure). 2-fold, 5-fold, and 10-fold dilution of samples did not significantly change the Rg, Dmax, or DAMMIF reconstructions of SAXS data. Comparisons of the SAXS reconstructions to the MiroS crystal structures were made with DAMAVER [47], SUPCOMB [48], and CRYSOL [49].

Size exclusion chromatography with multi-angle light scattering (SEC-MALS). Solution SEC-MALS experiments were conducted using Agilent Technologies 1200 LC HPLS system (Agilent Technologies, Santa Clara, CA) equipped with a Wyatt Dawn® Heleos™II 18-angle MALS light scattering detectors, Optilab® T-rEX™ (refractometer with EXtended range) refractive index detector, WyattQELS™ quasi-elastic (dynamic) light scattering (QELS) detector and ASTRA software (Wyatt Technology Europe GmbH, Dernbach, Germany). MiroS and MiroL proteins in SAXS buffer were buffer exchanged into SEC-MALS buffer (25 mM HEPES at pH 7.4, 300 mM NaCl, 0.5 mM TCEP, 0.5 mM EGTA + 1 mM $MgCl_2$ + 20 μM GTP) using a Superdex 200 (S200) 10/300 GL column (GE Healthcare, Piscataway, NJ), spin concentrated to 0.5-1.3 mg/mL and cleared of aggregates by ultracentrifugation. A total of 200 μL of MiroS or MiroL was injected and run on the S200 column at a flow rate of 0.5 mL/min in SEC-MALS buffer at 10 °C. The same procedure was repeated for the Ca^{2+}-containing samples using SEC-MALS buffer supplemented with 3 mM $CaCl_2$. Bovine serum albumin (BSA) was run as a control in both Ca^{2+}-free and 3 mM Ca^{2+} SEC-MALS buffers, and a void volume of 7.8 mL was determined using blue dextran (Sigma-Aldrich Corp., St. Louis, MO).

Funding support information for work conducted at the APS. Use of the Advanced Photon Source, an Office of Science User Facility operated for the U.S. Department of Energy (DOE)

Office of Science by Argonne National Laboratory, was supported by the U.S. DOE under Contract No. DE-AC02-06CH11357. Use of the LS-CAT was supported by the Michigan Economic Development Corp. and the Michigan Technology Tri-Corridor (085P1000817). Use of Bio-CAT was supported by grants from the National Center for Research Resources (2 P41RR008630-17) and the National Institute of General Medical Sciences (9 P41 GM103622-17) from the National Institutes of Health. The content is solely the responsibility of the authors and does not necessarily reflect the official views of the National Center for Research Resources, National Institute of General Medical Sciences or the National Institutes of Health.

SUPPLEMENTARY FIGURE LEGENDS

Supplementary Figure S1 | MiroS sequence alignment and structures. (**A**) Sequence alignment of *Drosophila* Miro (Dm Miro), human Miro 1 (Hs Miro1), and *Saccharomyces cerevisciae* Gem1p, a closely related protein in yeast. Identical residues are shown in red, similar residues in pink. Human Miro 1 and Gem1p are 32.6% identical, 50.9% similar. Structural elements, as defined in **B** and in the text, are shown in bars below the sequence. Note that in all of these proteins, the hydrophobic residues that form the interhelical contacts within both cEF/hEF hand pairs and the LM1 and LM2 helices are well conserved, and the Lnk1 and Lnk2 linkers are of similar length. Many residues within the EF hand/cGTPase interface are also highly conserved, as described in the text. (**B**) Top, superposition of all three MiroS structures reported in this work: apo-MiroS, Ca-MiroS, and MgGDP-MiroS (rmsd < 0.7 Å over 404 residues). This view of MiroS is referred to as the “side-view” in the text. Structural elements and their residues are as follows: nGTPase 1-200 (gray/white), cEF1 209-243 (dark blue), hEF1 249-287 (light blue), LM1 290-301 (bright blue), ELM1 209-301 (blue region), Lnk1 302-328 (orange), cEF2 329-360 (dark green), hEF2 368-401 (light green), LM2 403-413 (bright green), ELM2 329-413 (green region), Lnk2 414-445 (red), cGTPase 446-617 (gray/yellow), M (transmembrane domain) 618-652 (black/white). Note that although cEF1 and cEF2 are separated by hEF1, LM1, and Lnk1 in sequence, they are adjacent to one another in the structure at the ELM1/ELM2 interface. Center, “top-view”, 90° rotation from the side-view. In this view, the β-scaffold-stabilized EF hand loops are in the forefront, all on the same face of the molecule. Bottom, “bottom-view”, 180° rotation from the top-view. In this view, the linkers Lnk1 and Lnk2 and the ligand mimics LM1 and LM2, are in the forefront. EF hands are named αA/λ1/αB, αC/λ2/αD in order, according to convention [15]. The two linkers between the three

ELM1, ELM2, and cGTPase domains are named Lnk1 and Lnk2. β-sheets within the cGTPase are labeled Gβ1-6, α-helices Gα1-4, and loops GL1-7. Conserved GTPase motifs (P loop, SwI = Switch I, SwII = Switch II, G4 and G5, as defined by Bourne [17]) are also labeled. Structural elements are labeled with the same color as in the sequence diagram in **A**. Note that the Ca-MiroS structure was obtained by Ca^{2+}-soaks of MiroS crystal grown in the presence of EGTA, as described in supplementary Methods. This structure is virtually identical to the SeMet-MiroS structure obtained when MiroS was purified in the absence of any additional Ca^{2+} in the buffers and crystallized in the absence of EGTA. Both Ca-MiroS and SeMet-MiroS have electron density in cEF2 consistent with a Ca^{2+} ion. The Ca^{2+} present in the SeMet-MiroS structure is presumably bound from purification. We chose to present the Ca-MiroS structure here, because the electron density for Ca^{2+} in the Ca-MiroS structure indicated the presence of Ca^{2+} at higher occupancy than in the corresponding SeMet-MiroS structure.

Supplementary Figure S2 | The Miro "ligand mimic" LM helices and ELM domains. (**A**) The Miro LM helices structurally resemble extrinsic ligands bound to EF hand pairs. Top left to right: Miro ELM1 (blue), Miro ELM2 (green), overlay of "open" calmodulin N-lobe bound to two Ca^{2+} ions (white; PDB 1CLL [50]) and "closed" apo calmodulin N-lobe (black; PDB 1CFD [51]), Troponin C N-lobe bound to two Ca^{2+} ions (pink) bound to the Troponin I switch helix (red) (PDB 1YTZ [18]), and the "semi-open" apo myosin essential light chain C-terminal EF hand pair (ELC, pink) bound to myosin heavy chain (MHC, red) (PDB 1WDC [19]). All EF hands are shown in the orientation indicated for calmodulin (center), with αA lower left, αB upper left, αC upper right, and αD lower right. Ligand mimics or ligands are positioned horizontally. Table of angles between helix A and B (αA → αB) and helix A and C (αA → αC) for the structures

pictured above, indicates that the relative positions of the EF hand helices in both of Miro's ELM domains fall in between the open Ca^{2+}-bound, and closed apo conformations of calmodulin. Thus, both Miro ELM domains are in a 'semi-open' conformation, though their helical angles deviate somewhat from the semi-open structure of the myosin ELC C-terminal lobe [19]. (**B**) ELM and ELM-like domains seen in other proteins. EF hands are shown in pink, ligand mimics are shown in purple, extrinsic ligands in red. Left to right, polcalcin (PDB 1H4B [52], myristoylated apo recoverin (PDB 1IKU [25]), recoverin bound to rhodopsin kinase, showing both a C-terminal ligand mimic and an N-terminal extrinsic ligand (PDB 2I94 [31]), and guanylate cyclase activating protein 3, which contains an extended C-terminal ligand mimic for two EF hand pairs (GCAP; PDB 2GGZ [53]). Other proteins with ELM-like domains (not shown) include the plant NADPH oxidase OsRbohB, containing an ELM domain variant in which an N-terminal helix serves as an extended ligand mimic for two domain-swapped EF hand pairs (PDB 3A8R [54]), and neuronal calcium sensor, related to the recoverin family of proteins (PDB 1G8I [16]). The recoverin structures in particular demonstrate that ligand mimics can be displaced from EF hands in favor of extrinsic ligands. The structures indicate that recoverin's myristoylated N-terminal ligand mimic is buried in the Ca^{2+}-free N-terminal EF hand pair, but is replace by a helix from rhodopsin kinase when bound to Ca^{2+}.

Supplementary Figure S3 | Fo-Fc omit electron density map of the unidentified ligand (UNL). The map is contoured at 3.0σ with a cover radius of 7 Å about the UNL molecule, modeled as homoserine and shown in sticks.

Supplementary Figure S4 | 2Fo-Fc electron density maps, contoured at 1.3σ, at the EF hand loops regions, shown in the same orientation as in Fig 3.

Supplementary Figure S5 | The unidentified ligand (UNL) and/or crystal packing interactions may prevent Ca^{2+}-binding at cEF1. (**A**) Overlay of ELM1 and Ca^{2+}-bound ELM2 from the Ca-MiroS structure. The α-carbons of the ELM2 domain were aligned with the α-carbons of the αA1 helix and beginning of the cEF1 loop (ELM1 residues 217-236, rmsd 0.646 Å over 17 α-carbon pairs). αB1 in ELM1 is displaced relative to the position of αB2 in ELM2, likely due to the presence of the UNL (modeled here as homoserine, colored blue and shown as sticks inside the blue ELM1 core, encased in mesh corresponding to its 2Fo-Fc electron density maps, contoured at 1.2σ). The displacement is 1.0 Å at the α-carbon position of E234 (ELM1) relative to E354 (ELM2), increasing down the helix to 2.3 Å at the α-carbon of F238 (ELM1) relative to L358 (ELM2). (**B**) Crystal packing interactions cover up a "hole" in the ELM1 hydrophobic core. Lnk2 (red) from a crystallographic symmetry-mate forms a crystal packing contact with ELM1, involving Lnk2 hydrophobic residues I435 and L437 (orange). ELM1 is shown as a ribbon (colored as in Fig 1), with its surface shown around it (gray). The UNL is shown in stick representation as homoserine in the interior of ELM1. Mesh corresponds to 2Fo-Fc electron density maps contoured at 1.7σ.

Supplementary Figure S6 | Comparison of MiroS cGTPase domain with Rho and Ras structures. Left, overlay of RhoA (pink, PDB 1FTN [55]) with MiroS (gray with nucleotide-sensing motifs shown yellow) (rmsd 2.7 Å over 177 Cα positions). The Rho insert domain after the G4 loop is missing from the Miro cGTPase. Note that the cGTPase GL5 loop that

corresponds to the Rho insert domain contained high B-factors, as described in supplementary Methods. Center, overlay of Ras (green, PDB 4Q21 [56]) with MiroS (rmsd 2.7 Å over 168 Cα positions). Right, the Ras homolog Rheb (blue, PDB 1XTQ [24]) (rmsd 1.9 Å over 169 Cα positions). The structural alignment algorithm Dali [42] found Rheb to be the most similar GTPase to the Miro cGTPase in the PDB.

Supplementary Figure S7 | Solution SAXS studies of MiroS. **(A)** SAXS data for MiroS-Ca in 3 mM Ca^{2+}. From top to bottom, the scattering curve, Guinier plot, particle distribution function, and Kratky plot are shown. The scattering curve is Log(Intensity) vs. scattering angle (q). Raw data is shown as black dots with error bars representing the variability between exposures. The CRYSOL fit is in red and the predicted scattering intensity based on the DAMMIF reconstruction in blue. The Guinier plot (log(I) vs. q^2) is shown with linear fit for radius of gyration (Rg) measurement, which is $(3*slope)^{0.5}$. The particle distribution function P(r) indicates maximum diameter (Dmax). Kratky plots show clear maxima, indicating qualitatively that MiroS is well folded under these conditions. **(B)** Reconstructions based on MiroS SAXS data. The DAMAVER average of the DAMMIF runs is shown in gray, the DAMFILT filtered envelope is shown in magenta, and the MiroS MgGDP crystal structure, fit into the filtered envelope using SUPCOMB, is shown in black. From top to bottom, the views are the same as in supplementary Fig S1B. **(C)** and **(D)** similar SAXS data and reconstruction views for MiroS-Ca+MgGDP. **(E)** and **(F)** MiroS-Ca+MgGTP.

Supplementary Figure S8 | Scattering curves and Guinier plots of MiroS under Ca^{2+}-free conditions. Data for Miro in the absence of Ca^{2+} was not of sufficient quality to yield good

reconstructions, but Rg could still be determined from the Guinier plots. **(A)** MiroS-apo. **(B)** MiroS-Mg. **(C)** MiroS-MgGDP. Accompanying data is shown in supplementary Table S2.

Supplementary Figure S9 | SEC-MALS studies of Miro. SEC-MALS data for both the crystallized MiroS fragment and MiroL (aa 1-617; MiroL has both the N-terminal and C-terminal GTPase domains). Both proteins are monomeric in solution. Typical SEC UV λ_{280} (A280) absorbance profiles are shown, normalized for each run (y-axis on left). In-line MALS-determined molecular weights (MWs) were calculated over the entire SEC run and the MW profiles across each elution peak are shown (y-axis on right). MALS-determined MWs are as follows: MiroL No Ca^{2+} (71.23 ± 0.71 kD), MiroL 3 mM Ca^{2+} (70.91 ± 0.21 kD), MiroS No Ca^{2+} (49.57 ± 0.50 kD), MiroS 3 mM Ca^{2+} (48.87 ± 0.49 kD). Calculated MWs based on protein sequence are: MiroL (71.008 kD) and MiroS (49.047 kD). Protein concentrations were as follows: MiroL no Ca^{2+} (0.5 mg/mL), MiroL 3 mM Ca^{2+} (0.7 mg/mL), MiroS no Ca^{2+} (1.1 mg/mL), MiroS 3 mM Ca^{2+} (1.3 mg/mL). The void volume was ~7.8 mL, and the total column volume was ~20 mL.

Supplementary Table S1 | Crystallographic refinement statistics for MiroS structures.

Supplementary Table S2 | SAXS parameters and errors. Rg and error in Rg were calculated from weighted linear regression analysis of Guinier curves from raw SAXS data (see supplementary Figs S7-S8). Reported Dmax values were determined using GNOM. In determining Dmax, GNOM gives a “total estimate”, which identifies common artifacts encountered by the GNOM method. Good/reasonable total estimates indicate that commonly

observed errors were not made in determining Dmax for our datasets. Scattering data of apo MiroS and MiroS in the presence of Mg^{2+} but not Ca^{2+} or GTP (MiroS-Mg) (supplementary Fig S8) showed evidence of unfolded/unstable protein in the high and low Q range of scattering curves. While these data were of sufficient quality to obtain Rg, the calculated Dmax value in the case of apo MiroS was large (121 Å) and a single Dmax could not produce a satisfactory P(r) curve for MiroS-Mg or MiroS-MgGDP in GNOM. Therefore, these datasets were not used for DAMMIF reconstructions. Like other EF hand proteins, Miro may be less stable in the absence of Ca^{2+} [14,21]. For MiroS-Ca, MiroS-Ca+GDP, and MiroS-Ca+GTP, alignment of SAXS and crystal structure data was performed using SUPCOMB [48]. The normalized spatial discrepancy (NSD) is a measure of the quantitative similarity between the different independent runs of DAMMIF. The reported NSD values indicate that the DAMMIF reconstructions are very stable. χ^2 values compare theoretical scattering data based on DAMMIF reconstructions and CRYSOL crystal structure fits to our actual scattering data. These were calculated as described in [49]. DAMMIF reconstructions yielded a good model of the SAXS data throughout the entire Q range. CRYSOL fits matched the SAXS data over a Q range of 0.01-0.14 with reasonable χ^2 values, then deviated significantly from experimental data at higher Q. This indicates that these solution structures of Miro differ significantly from the crystal structure on length scales < 7-10 Å, a possible indication of protein flexibility on that length scale.

Supplementary Figure S1

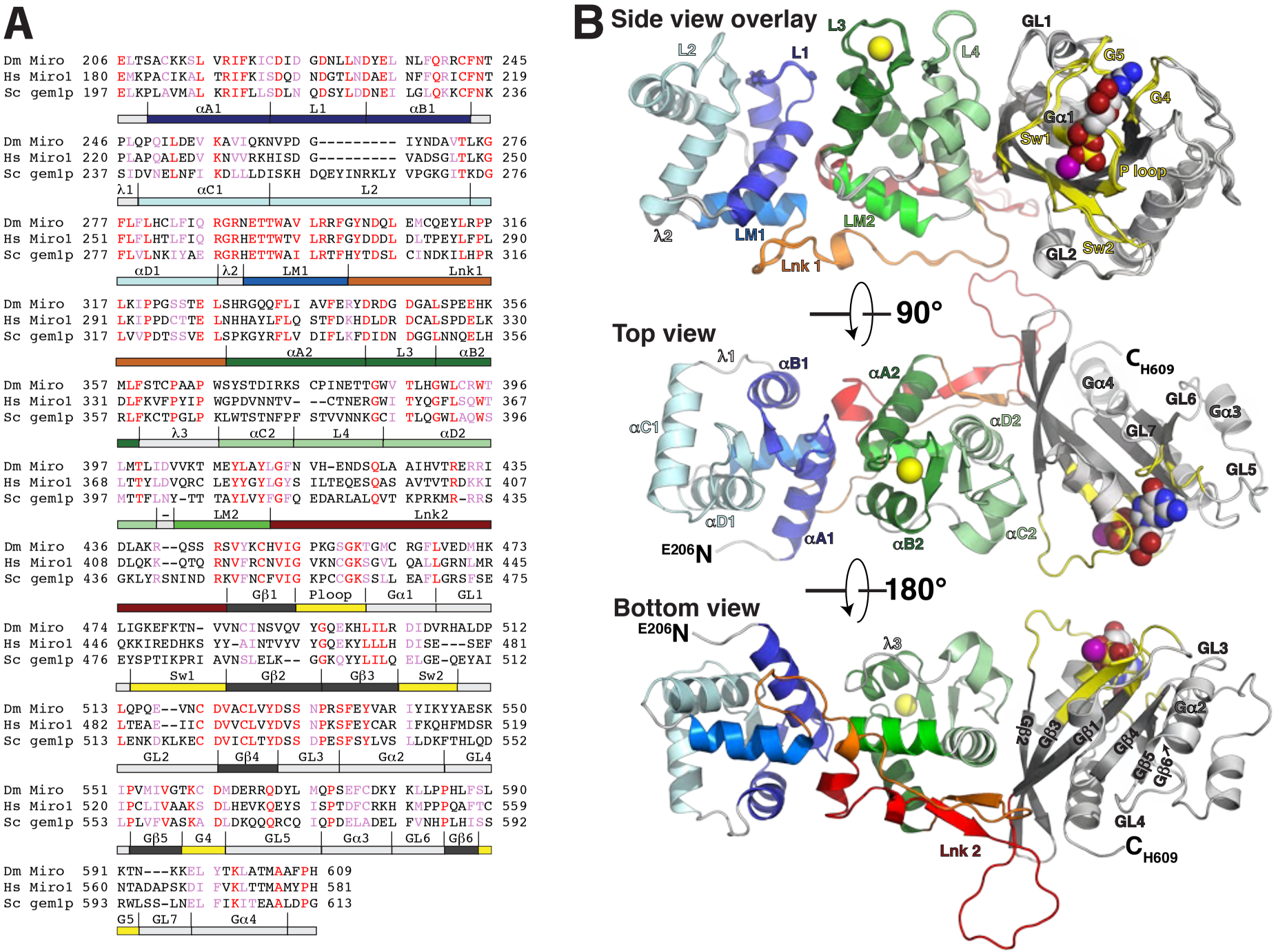

Supplementary Figure S2

A

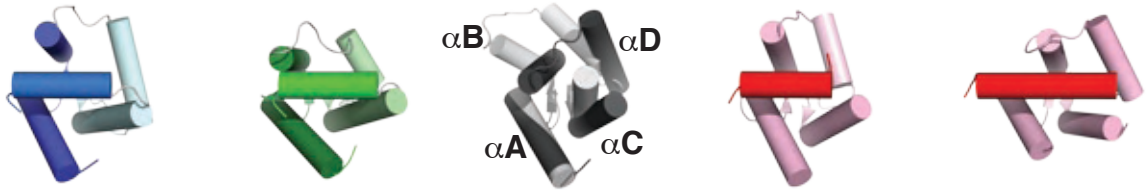

EF Hand	ELM1	ELM2	CaM open	CaM closed	TnC/TnI open	ELC/MHC semi-open
αA->αB	123°	123°	89°	136°	105°	126°
αA->αC	123°	119°	163°	95°	151°	104°

B

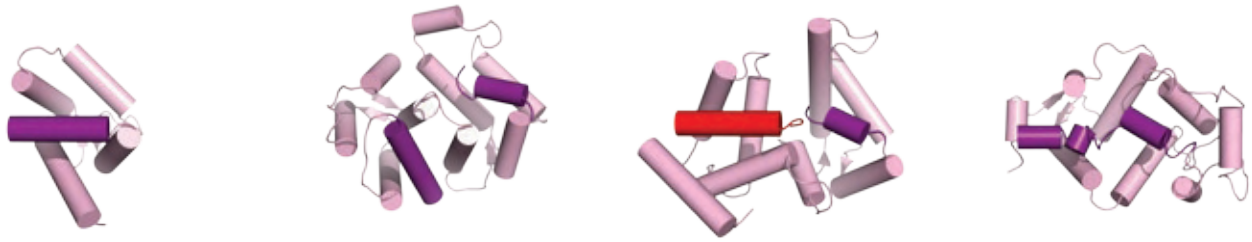

polcalcin | recoverin | recoverin/ rhodopsin kinase | GCAP

Supplementary Figure S3

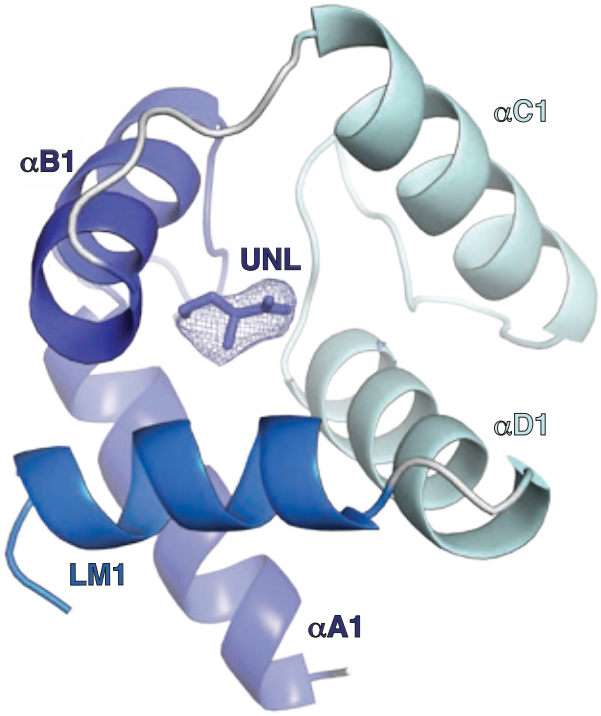

Supplementary Figure S4

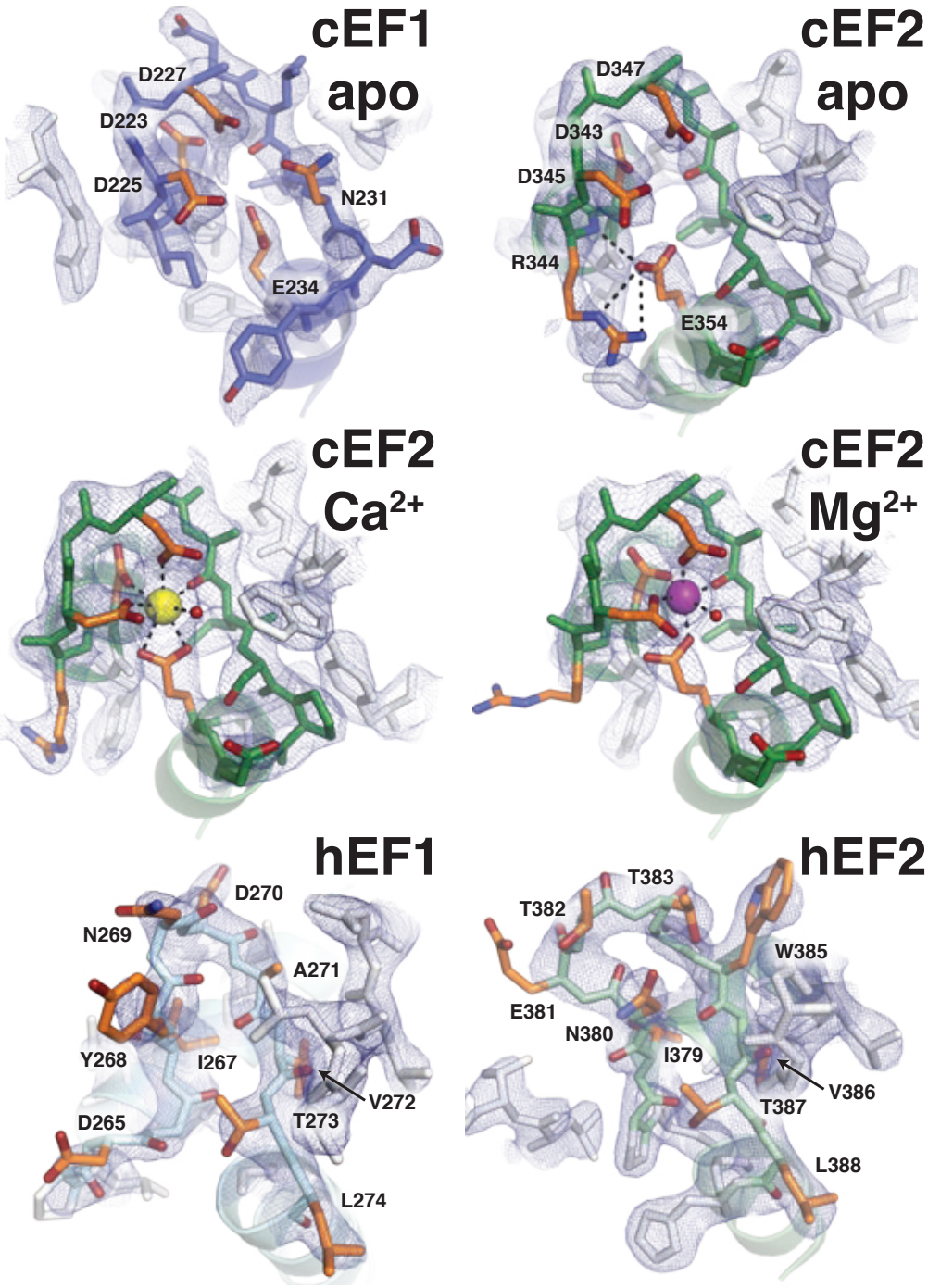

Supplementary Figure S5

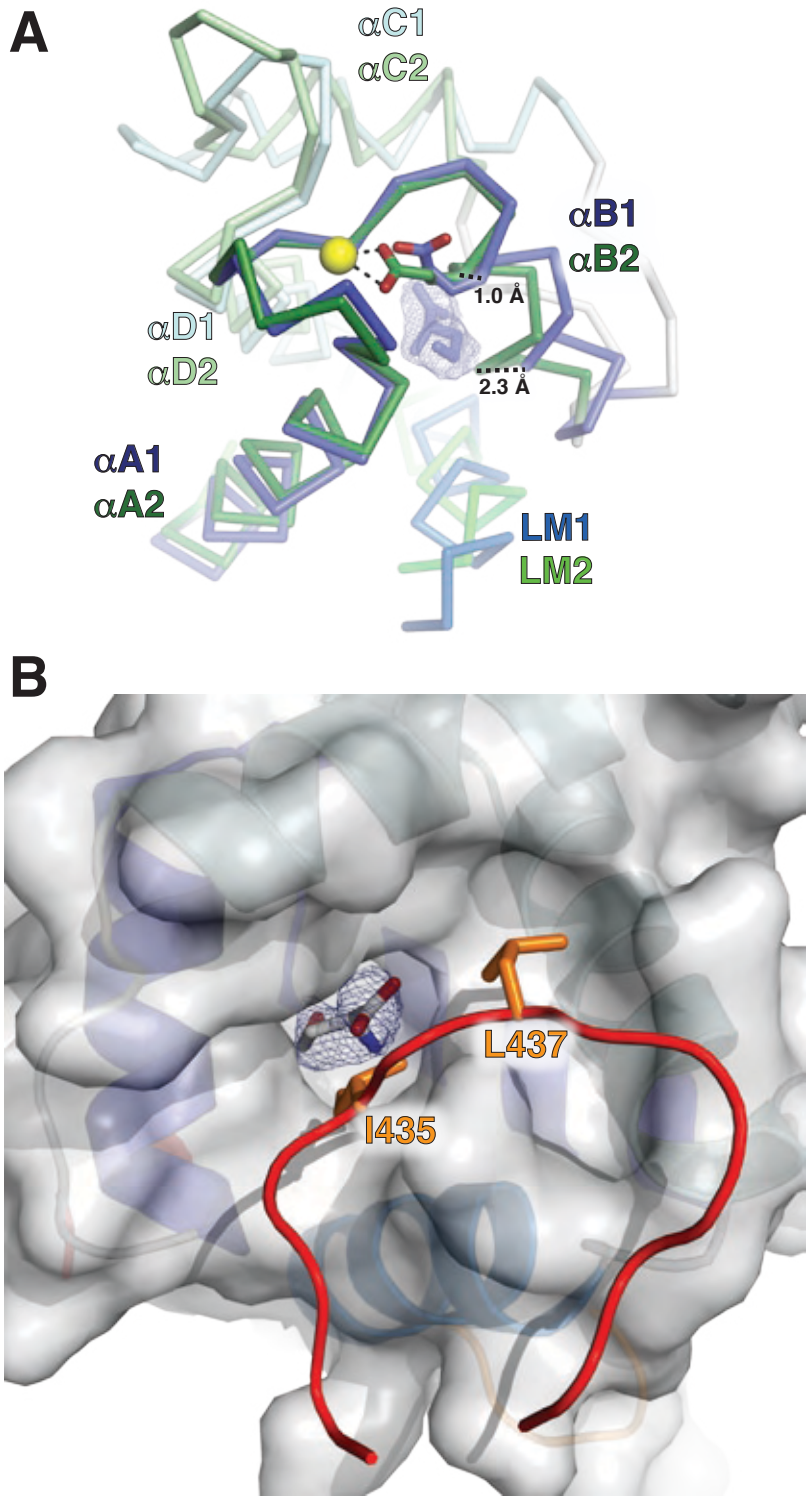

Supplementary Figure S6

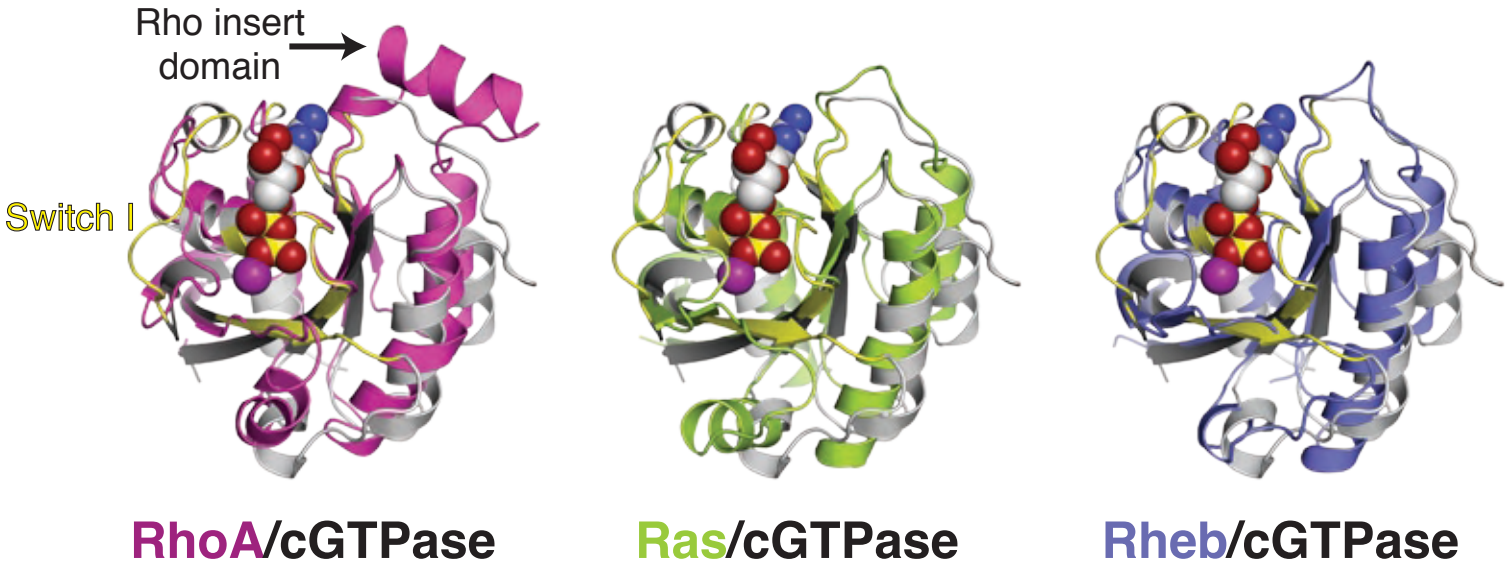

MiroS-Ca

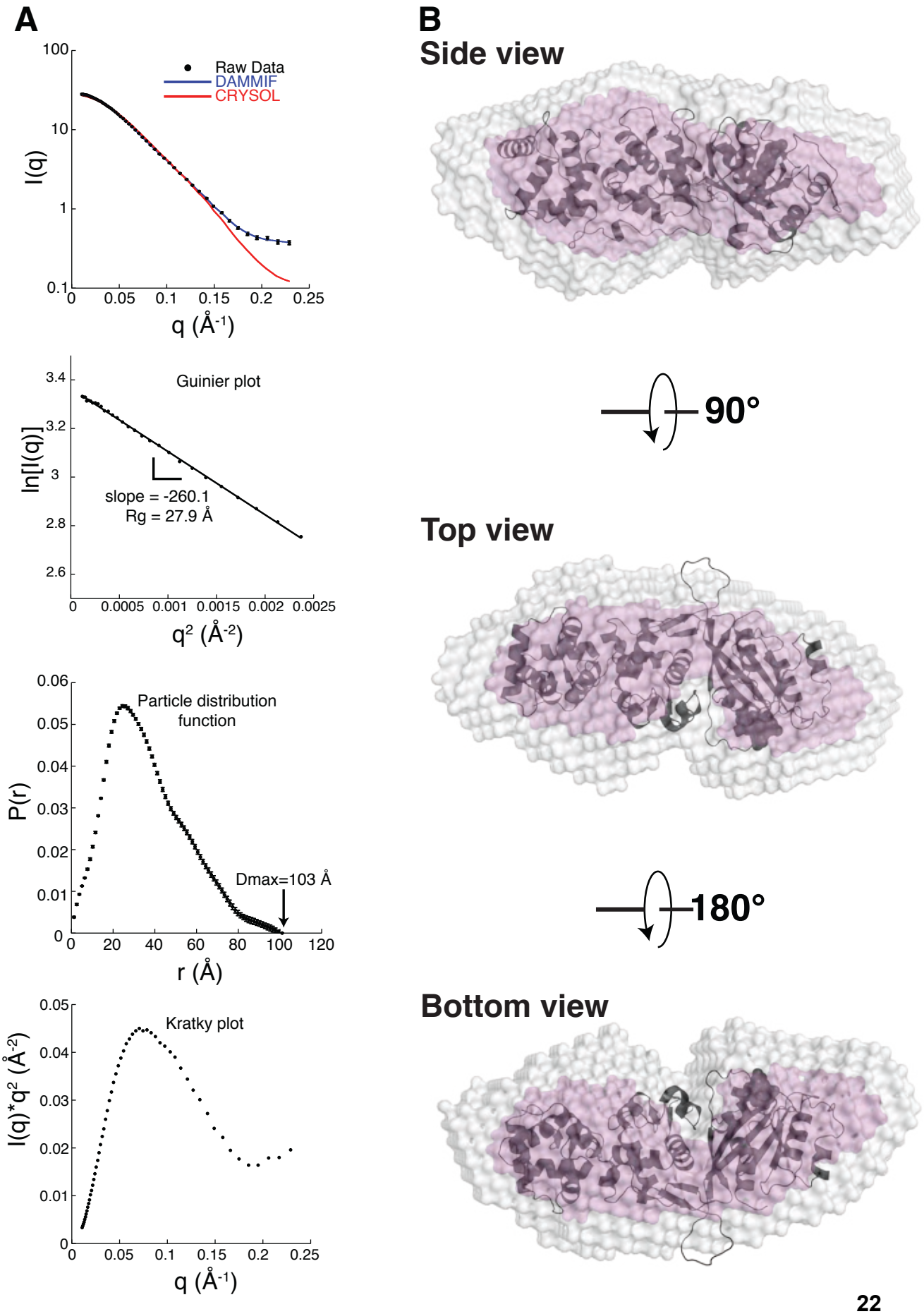
A
Raw Data
DAMMIF
CRYSOL
I(q)
q (Å-1)
Guinier plot
ln[I(q)]
slope = -260.1
Rg = 27.9 Å
q2 (Å-2)
Particle distribution function
P(r)
Dmax=103 Å
r (Å)
Kratky plot
I(q)*q2 (Å-2)
q (Å-1)
B
Side view
90°
Top view
180°
Bottom view

MiroS-Ca+MgGDP

C

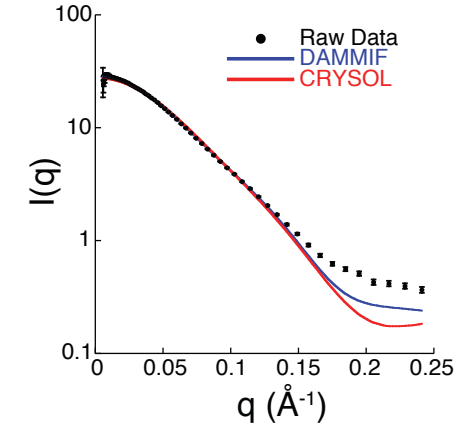

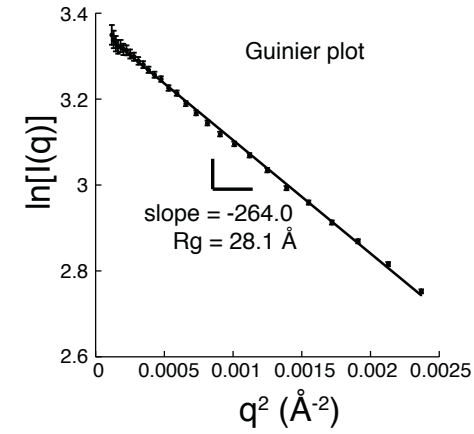

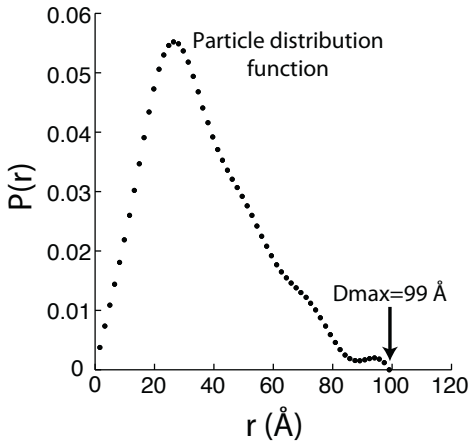

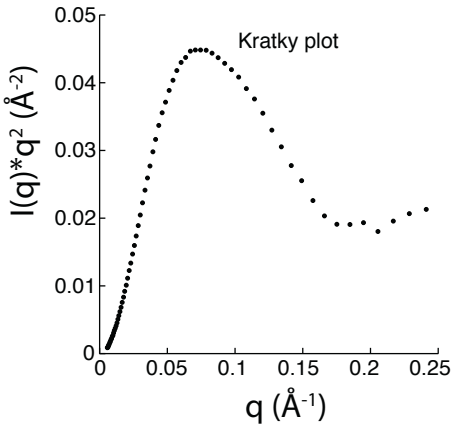

D

Side view

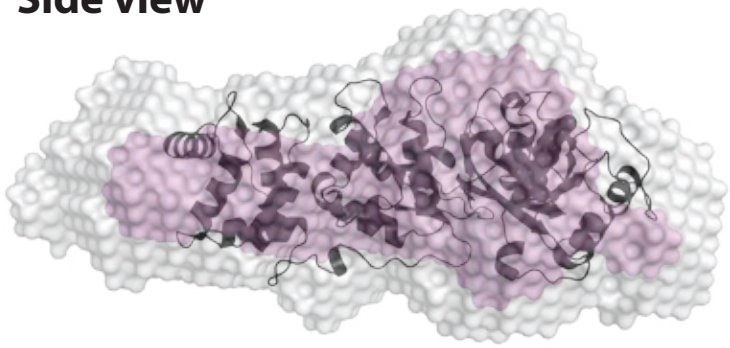

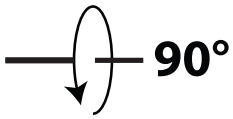

Top view

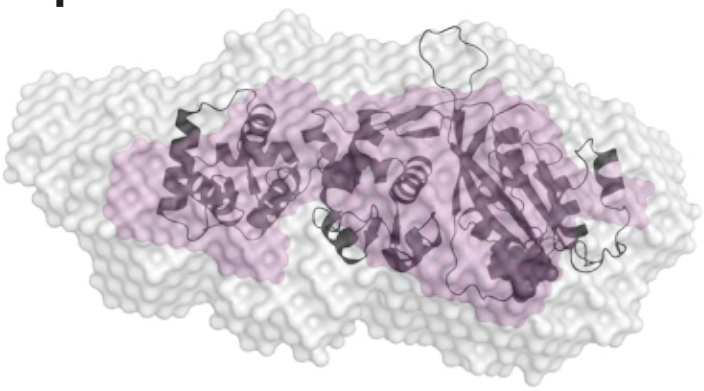

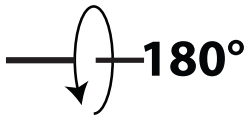

Bottom view

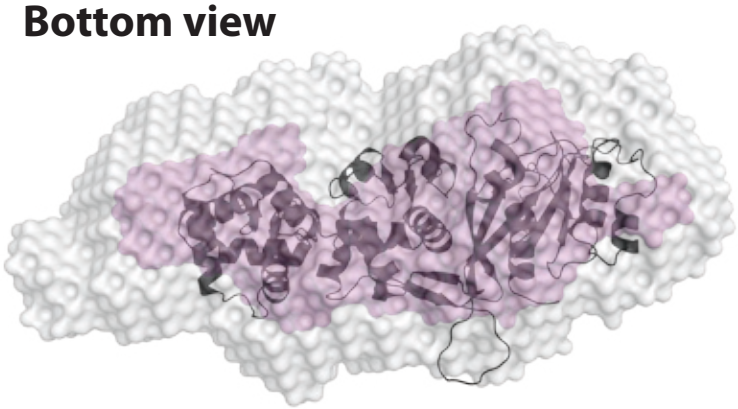

MiroS-Ca+MgGTP

E

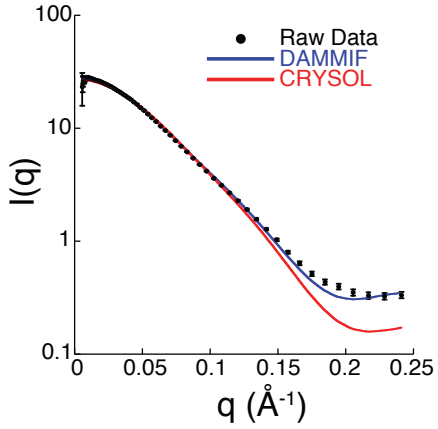

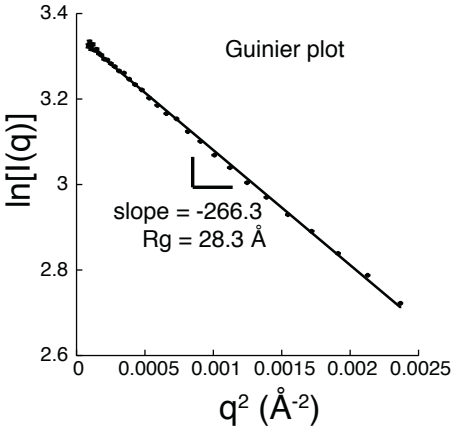

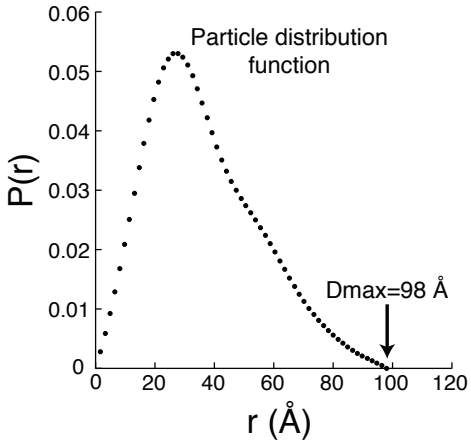

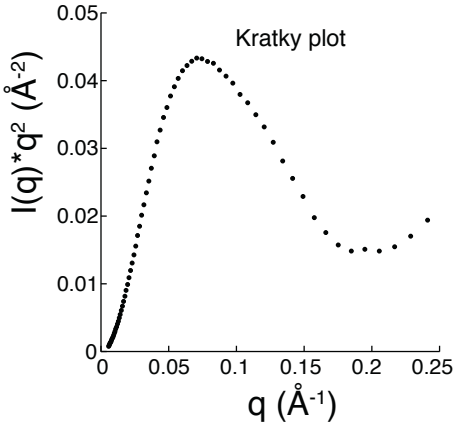

F

Side view

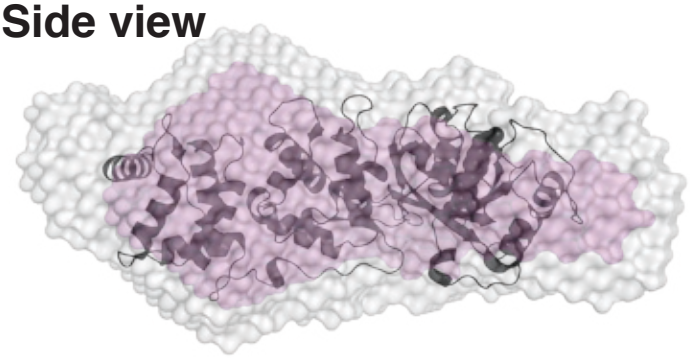

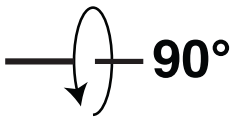

Top view

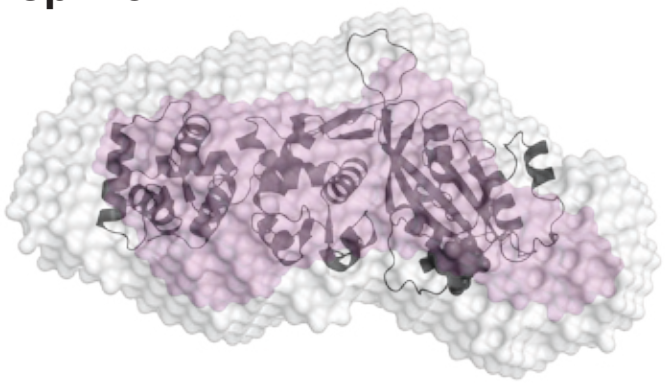

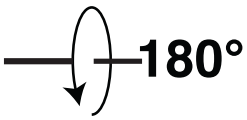

Bottom view

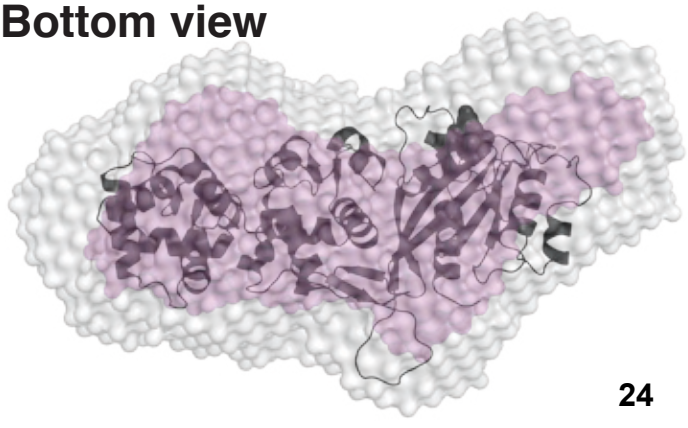

Supplementary Figure S8

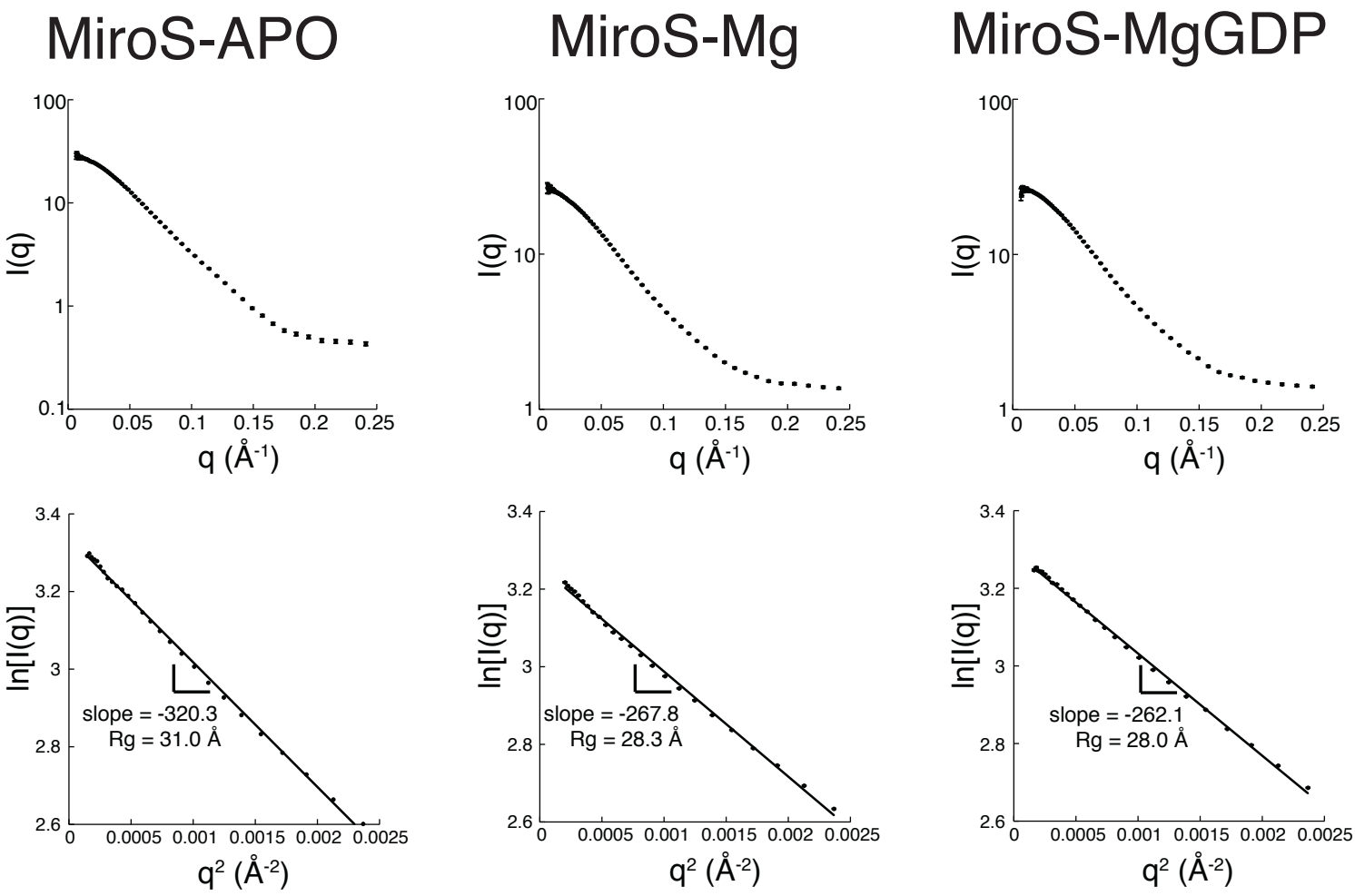

Supplementary Figure S9

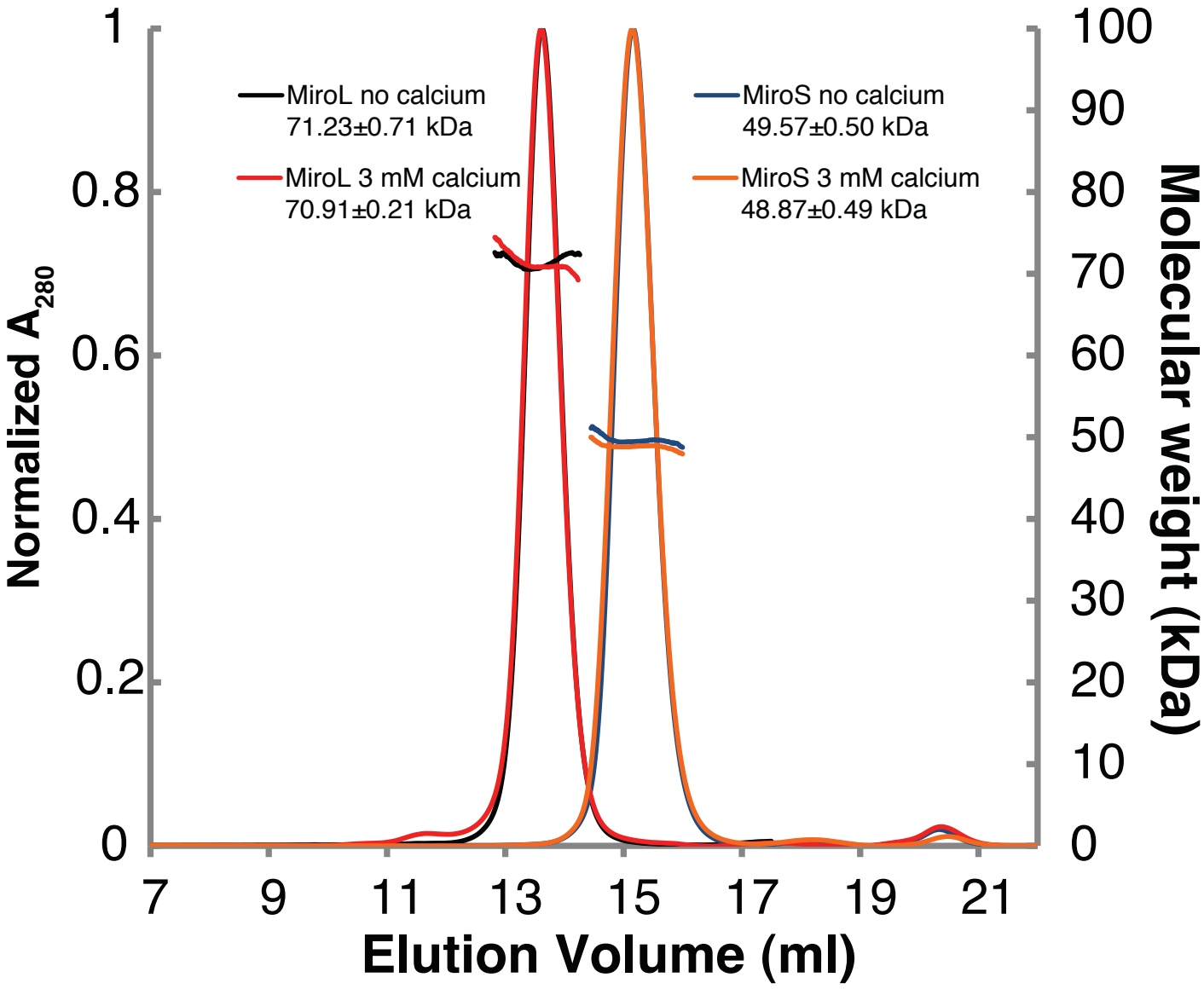

Supplementary Table S1

Crystallographic Statistics				
Data Collection	SeMet-MiroS	apo-MiroS	Ca-MiroS	MgGDP-MiroS
Space group	$P3_221$	$P3_221$	$P3_221$	$P3_221$
Unit cell parameters:				
a, b, c (Å)	82.58, 82.58, 156.38	81.93, 81.93, 155.82	82.24, 82.24, 156.44	81.51, 81.51, 154.95
α, β, γ (°)	90, 90, 120	90, 90, 120	90, 90, 120	90, 90, 120
Resolution range	29.5-2.61 (2.64-2.61) [a]	41.9–2.82 (2.99-2.82)	42.1-2.80 (2.97-2.80)	52.2-3.00 (3.24-3.00)
Unique reflections	19410 (974) [a]	15216 (2399)	15693 (2482)	12487 (2511)
[b] R_{merge}	0.096 (0.708) [a]	0.097 (0.589)	0.135 (0.696)	0.079 (0.575)
Completeness (%)	100 (100)	100 (100)	100 (100)	100 (100)
Multiplicity	10.8 (10.8)	14.6 (13.1)	15.1 (15.5)	6.6 (6.7)
Mean I/σ(I)	22.9 (2.3)	16.6 (3.5)	11.1 (1.6)	11.8 (2.4)
Phasing				
Number of Se sites	10			
Figure of Merit (acentric/centric)	0.431/0.112			
# Reflections (acentric/centric)	10320/2263			
Refinement				
Resolution range [a]	29.5 - 2.61 (2.70-2.61) [a]	34.6 - 2.82 (2.92-2.82)	42.1 - 2.80 (2.90-2.80)	25.8 - 3.00 (3.11-3.00)
[e] R_{cryst}	0.1916 (0.2283) [a]	0.2247 (0.3075)	0.2072 (0.3406)	0.2145 (0.3582)
R_{free}	0.2651 (0.3045)	0.2617 (0.3532)	0.2422 (0.3985)	0.2585 (0.4078)
Number of atoms	3403	3320	3325	3317
Protein	3247	3231	3225	3245
Ligands	24	30	31	55
Solvent	132	59	69	17
RMS bonds (Å)	0.010	0.002	0.002	0.002
RMS angles (°)	1.27	0.53	0.48	0.52
Average B-factor (Å^2)	21.1	36.5	47.6	62.1
Protein	21.2	36.5	47.7	61.9
Ligands	30.1	49.1	56.6	78.2
Solvent	16.5	29.4	37.7	43.8
Ramachandran Plot Regions				
Favored (%)	94	96	97	96
Outliers (%)	1.7	0.25	0.25	0
PDB ID code		4c0j	4c0k	4c0l

[a] Values in parentheses correspond to the highest resolution shell

[b] $R_{merge} = \Sigma_{hkl}\Sigma_i|I(hkl)_i - \langle I(hkl)\rangle|/\Sigma_{hkl}\Sigma_i\langle I(hkl)_i\rangle$

[e] $R_{cryst} = \Sigma_{hkl}|F(hkl)_o - F(hkl)_c|/\Sigma_{hkl}|F(hkl)_o|$; R_{free} is calculated for 10% of the data omitted from the refinement.

Supplementary Table S2

Dataset	MiroS-Ca	MiroS-Ca+MgGDP	MiroS-Ca+MgGTP	MiroS-apo	MiroS-Mg	MiroS-MgGDP
Rg (Å)	27.9 ± 0.1	28.1 ± 0.1	28.3 ± 0.1	31.0 ± 0.06	28.3 ± 0.2	28.0 ± 0.1
Dmax (Å)	103	99	98	121	N.D.	N.D.
Total estimate from GNOM	0.854 (Good)	0.860 (Good)	0.662 (Reasonable)	0.581 (Reasonable)	N.D.	N.D.
NSD of DAMMIF reconstructions	0.82 ± 0.04	0.93 ± 0.04	0.79 ± 0.06	0.742 ± 0.056	N.D.	N.D.
DAMMIF χ^2	0.35	0.29	0.49	0.40	N.D.	N.D.
CRYSOL χ^2 (Q=0.01-0.14)	0.62	0.43	0.64	N.D.	N.D.	N.D.

SUPPLEMENTARY REFERENCES

32. Van Duyne GD, Standaert RF, Karplus PA, Schreiber SL, Clardy J (1993) Atomic structures of the human immunophilin FKBP-12 complexes with FK506 and rapamycin. *J Mol Biol* **229**: 105–24

33. Otwinowski Z, Minor W (1997) Processing of X-ray Diffraction Data Collected in Oscillation Mode. *Methods Enzymol* **276**: 307–26

34. Evans PR (2011) An introduction to data reduction: space-group determination, scaling and intensity statistics. *Acta Crystallogr D* **67**: 282–92

35. Adams PD, Afonine PV, Bunkóczi G, Chen VB, Davis IW, Echols N, Headd JJ, Hung L-W, Kapral GJ, et al. (2010) PHENIX: a comprehensive Python-based system for macromolecular structure solution. *Acta Crystallogr D* **66**: 213–21

36. Emsley P, Lohkamp B, Scott WG, Cowtan K (2010) Features and development of Coot. *Acta Crystallogr D* **66**: 486–501

37. McCoy AJ, Grosse-Kunstleve RW, Adams PD, Winn MD, Storoni LC, Read RJ (2007) Phaser crystallographic software. *J. Appl. Cryst* **40**: 658–74

38. Afonine PV, Grosse-Kunstleve RW, Adams PD (2005) A robust bulk-solvent correction and anisotropic scaling procedure. *Acta Crystallogr D* **61**: 850–5

39. Laurie ATR, Jackson RM (2005) Q-SiteFinder: an energy-based method for the prediction of protein-ligand binding sites. *Bioinformatics* **21**: 1908–16

40. Vangone A, Spinelli R, Scarano V, Cavallo L, Oliva R (2011) COCOMAPS: a web application to analyze and visualize contacts at the interface of biomolecular complexes. *Bioinformatics* **27**: 2915–6

41. DeLano W (2002) The PyMOL Molecular Graphics System.

42. Holm L, Rosenström P (2010) Dali server: conservation mapping in 3D. *Nucleic Acids Res* **38**: W545–9

43. Goujon M, McWilliam H, Li W, Valentin F, Squizzato S, Paern J, Lopez R (2010) A new bioinformatics analysis tools framework at EMBL-EBI. *Nucleic Acids Research* **38**: W695–9

44. Fischetti R, Stepanov S, Rosenbaum G, Barrea R, Black E, Gore D, Heurich R, Kondrashkina E, Kropf AJ, et al. (2004) The BioCAT undulator beamline 18ID: a facility for biological non-crystalline diffraction and X-ray absorption spectroscopy at the Advanced Photon Source. *Journal of synchrotron radiation* **11**: 399–405

45. Svergun DI (1992) Determination of the regularization parameter in indirect-transform

methods using perceptual criteria. *J. Appl. Cryst* **25**: 495–503

46. Franke D, Svergun DI (2009) DAMMIF, a program for rapid ab-initioshape determination in small-angle scattering. *J. Appl. Cryst* **42**: 342–6

47. Volkov VV, Svergun DI (2003) Uniqueness of ab initioshape determination in small-angle scattering. *J. Appl. Cryst* **36**: 860–4

48. Kozin MB, Svergun DI (2001) Automated matching of high-and low-resolution structural models. *J. Appl. Cryst* **34**: 33–41

49. Svergun D, Barberato C, Koch MHJ (1995) CRYSOL– a Program to Evaluate X-ray Solution Scattering of Biological Macromolecules from Atomic Coordinates. *J. Appl. Cryst* **28**: 768–73

50. Chattopadhyaya R, Meador WE, Means AR, Quiocho FA (1992) Calmodulin structure refined at 1.7 A resolution. *J Mol Biol* **228**: 1177–92

51. Kuboniwa H, Tjandra N, Grzesiek S, Ren H, Klee CB, Bax A (1995) Solution structure of calcium-free calmodulin. *Nat Struct Biol* **2**: 768–76

52. Neudecker P, Nerkamp J, Eisenmann A, Nourse A, Lauber T, Schweimer K, Lehmann K, Schwarzinger S, Ferreira F, et al. (2004) Solution Structure, Dynamics, and Hydrodynamics of the Calcium-bound Cross-reactive Birch Pollen Allergen Bet v 4 Reveal a Canonical Monomeric Two EF-Hand Assembly with a Regulatory Function. *J Mol Biol* **336**: 1141–57

53. Stephen R, Palczewski K, Sousa MC (2006) The Crystal Structure of GCAP3 Suggests Molecular Mechanism of GCAP-linked Cone Dystrophies. *J Mol Biol* **359**: 266–75

54. Oda T, Hashimoto H, Kuwabara N, Akashi S, Hayashi K, Kojima C, Wong HL, Kawasaki T, Shimamoto K, et al. (2010) Structure of the N-terminal regulatory domain of a plant NADPH oxidase and its functional implications. *J Biol Chem* **285**: 1435–45

55. Wei Y, Zhang Y, Derewenda U, Liu X, Minor W, Nakamoto RK, Somlyo AV, Somlyo AP, Derewenda ZS (1997) Crystal structure of RhoA-GDP and its functional implications. *Nat Struct Biol* **4**: 699–703

56. Milburn M, Tong L, deVos A, Brunger A, Yamaizumi Z, Nishimura S, Kim S (1990) Molecular switch for signal transduction: structural differences between active and inactive forms of protooncogenic ras proteins. *Science* **247**: 939–45.